Atmospheric
Chemistry
and Physics
Discussions

Open Access

1 Hygroscopic growth effect on aerosol light scattering in the urban area of

2 Beijing: a long-term measurement by a wide-range and high-resolution

3 humidified nephelometer system

4 **Pusheng Zhao[1*], Jing Ding[2, 1], Xiang Du[2, 1], and Jie Su[1]**

5 [1] Institute of Urban Meteorology, China Meteorological Administration, Beijing 100089, China

6 [2] State Environmental Protection Key Laboratory of Urban Ambient Air Particulate Matter Pollution

7 Prevention and Control, College of Environmental Science and Engineering, Nankai University,

8 Tianjin 300071, China

9 *Correspondence to:* P. S. Zhao (pszhao@ium.cn)

10

11 **Abstract:**
12 Hygroscopicity is an important feature of ambient aerosols, which is very crucial to the
13 study of light extinction, radiation force, and formation mechanism. The light scattering
14 hygroscopic growth factor (f(RH)) is an important parameter which is usually measured
15 by the humidified nephelometer system and could better describe the aerosol
16 hygroscopicity under wide particle size range and continuous relative humidity (RH).
17 The f(RH) can be applied to the establishment of a parameterization scheme for light
18 extinction, the calculation of hygroscopicity parameter (κ), and also the estimation of
19 aerosol liquid water content (ALWC). However, the humidified nephelometer system
20 in the previous studies could only observe the f(RH) below 90% due to the larger error
21 of the sensor under high RH (>90%). Furthermore, the f(RH) observations in North
22 China Plain needs to be greatly strengthened both in the temporal resolution and the
23 observation duration. In view of this, an improved high-resolution humidified
24 nephelometer system was established to observe the f(RH) of $PM_{2.5}$ for a wide RH range
25 between 30%-96% in the urban area of Beijing over three seasons (winter, summer, and
26 autumn) in 2017. It was found that the f(80%) at 525nm of $PM_{2.5}$ was evidently higher
27 under the polluted conditions and highly correlated with the fractions of all the water-
28 soluble ions. A two-parameter fit equation was selected to fit the observed f(RH) data.
29 For each season, the fitting curve under the very clean condition was lower than that of
30 other conditions. And the f(RH) points of polluted conditions were more concentrated
31 with higher fitting R^2 for summer and autumn data. The hygroscopicity of aerosol under
32 higher RH was probably enhanced when compared with the data in the previous study
33 conducted in NCP. In summer, the fitting f(RH) showed a significant dependence on
34 wavelength for each pollution condition. However, there was an opposite performance
35 in the f(RH) curves of different wavelengths for the very clean condition in winter. It
36 was shown that The simulation showed that the maximum uncertainty of f(RH) was
37 less than 10%.

Atmospheric
Chemistry
and Physics
Discussions

1. Introduction

38
39   Atmospheric aerosols influence the atmospheric visibility and earth-atmosphere
40   radiation budget directly by scattering and absorbing solar radiation (Charlson et al.,
41   1992; Schwartz et al., 1995; DeBell et al., 2006), and indirectly by modifying
42   microphysical properties and lifetime of clouds (Twomey, 1974; Albrecht, 1989;
43   Rosenfeld, 2000). The particle size, single scattering albedo (SSA), asymmetry
44   parameter (AP), and refractive index are the key parameters in estimating the aerosol
45   radiative forcing; and these parameters are strongly dependent on the relative humidity
46   (RH). Water uptake can result in enlarged particle sizes, SSA, and AP, change the
47   scattering phase functions, and decreased the refractive index (Cheng et al., 2008).
48   Moreover, numerous studies demonstrate that reaction in aerosol liquid water is an
49   important pathway of secondary aerosol formation, and thus plays a significant role in
50   the overall aerosol chemical composition (McMurry and Wilson, 1983; Ravishankara
51   1997; Kolb et al., 2010; Jang et al., 2002; Liu et al., 2012; Cheng et al., 2016).
52   Furthermore, water uptake is also important in the remote-sensing measurements or
53   satellite retrievals of aerosol optical properties (Wang and Martin, 2007; Zieger et al.,
54   2012).
55   Particle size and chemical composition are the main factors affecting the moisture
56   absorption ability of aerosol particles (Köhler, 1936; Hinds, 2011; Petters and
57   Kreidenweis, 2007; Seinfeld and Pandis, 2016). Particle size mainly affects the extent
58   of the Kelvin effect, while the chemical composition is the most crucial factor. Some
59   simulations demonstrated that the changes of aerosol size distribution could only lead
60   to slight variations in hygroscopic growth factor if the chemical compositions were
61   fixed (Fierz-Schmidhauser et al., 2010; Liu 2015; Kuang et al., 2017).
62   Generally, aerosol hygroscopicity could be described by the diameter growth factor
63   (g(RH)), light scattering hygroscopic growth factor (f(RH)), and hygroscopicity
64   parameter (κ). Size-resolved g(RH) could be directly measured by the Humidified
65   Tandem Differential Mobility Analyzer (HTDMA) (Liu et al. 1978; Swietlicki et al.,
66   2008). Due to the limitation of the HTDMA itself, only the particles with the dry
67   diameter under 350nm are usually observed. The f(RH) is calculated as the ratio of the
68   scattering coefficient at a certain RH to the corresponding dry scattering coefficient
69   (reference RH<40%), which can be measured by a dual nephelometer system (Covert
70   et al., 1972; Rood et al., 1985). In recent years, the κ-Köhler theory has been widely
71   used to describe the hygroscopic properties of aerosols (Petters and Kreidenweis, 2007),
72   in which all of the chemical composition dependent variables were merged into a
73   hygroscopicity parameter (κ). It facilitates the intercomparison of particle
74   hygroscopicity obtained by different equipment or different relative humidity. It is
75   applicable to both the single-component and the multicomponent aerosol particles.
76   Knowing the κ, dry diameter, and the relative humidity (RH), the g(RH) and liquid
77   water content (LWC) of aerosol particles could be calculated by using the κ-Köhler
78   equation.
79   The f(RH) synthetically reflects the impact of water uptake on aerosol particle size,
80   morphology, refractive index, etc., and consequently, on the scattering coefficient.
81   Firstly, the f(RH) results can be directly applied to the establishment of a

Atmospheric
Chemistry
and Physics
Discussions

82   parameterization scheme for light extinction. The parameterization scheme could be
83   built based on chemical compositions (DeBell et al., 2006; Pitchord et al., 2007), mass
84   concentrations (Chen et al., 2015), or volume concentrations (Chen et al., 2012, 2014).
85   No matter which scheme is used, the effect of relative humidity on extinction or
86   scattering coefficient must be taken into account. Secondly, the f(RH) could be used to
87   calculate the hygroscopicity parameter (κ) combining with the measurement of particle
88   number concentration size distributions (PNSD) (Chen et al., 2014; Kuang et al., 2017).
89   This κ does not target specific particle size but represents the overall hygroscopicity of
90   the observed aerosol. Thirdly, the f(RH) results derived from a three-wavelength
91   nephelometer system have also been used for the calculation of aerosol liquid water
92   content (ALWC) (Kuang et al., 2018) and number concentrations of cloud condensation
93   nuclei (Tao et al., 2018).
94   The humidified nephelometer system was firstly used by Pilat and Charlson (1966)
95   to measure the effect of humidity on the light scattering and the size of NaCl particles.
96   Covert et al. (1972) then used a similar system to study the hygroscopic and/or
97   deliquescence effects which were dependent upon relative humidity for pure particles.
98   Rood et al. (1985) improved the humidified nephelometers, which could control the RH
99   more precisely. In the past two decades, Carrico et al. (2000), Day et al. (2000),
100   Koloutsou-Vakakis et al. (2001), Fierz-Schmidhauser et al. (2010), Liu et al. (2016),
101   etc. further improved the humidified nephelometers to accurately measure the f(RH)
102   and study the light scattering enhancement characteristics of aerosol. While all the
103   humidified nephelometer system in the previous studies could only observe the f(RH)
104   below 90% RH because there would be a ±5% error in the RH measurement in the
105   optical chamber of nephelometer when the RH was humidified over 90%. However, for
106   a hygroscopic particle, its particle size or scattering cross section will increase sharply
107   when the relative humidity exceeds 90%. Accordingly, the results above 90% RH would
108   be quite important for f(RH) curve fitting and light scattering calculating.
109   As we all know, the North China Plain (NCP) is the most severe area of air pollution
110   in China. The aerosol hygroscopicity is an important basis for the studies of
111   atmospheric visibility, radiative forcing, and aerosol secondary formation in this area.
112   The HTDMA had been used in some campaigns in NCP (Massling et al., 2009; Meier
113   et al., 2009; Liu et al., 2011; Wang et al., 2018). As mentioned above, the g(RH)
114   observations using HTDMA had been basically limited to 350 nm, and could not be set
115   at multiple RH points. In comparison, the overall hygroscopicity of ambient aerosol at
116   several continuous RH points could be obtained by the f(RH) observation, which would
117   also be used to further calculate the hygroscopicity parameter and ALWC. In recent
118   years, the f(RH) observation has been carried out in only a few studies in NCP (Yan et
119   al., 2009; Pan et al., 2009; Chen et al., 2014; Kuang et al., 2017). In these studies, either
120   the temporal resolution of f(RH) was low, or the observation period was short. Moreover,
121   the f(RH) was limited to 90% RH in all these studies.
122   At present, some numerical pollution prediction systems have been established in the
123   region of NCP. However, the prediction of visibility is short of good means and methods.
124   Thus, an accurate, easy to use, and seasonal representative visibility parameterization
125   scheme is very critical and urgent. Furthermore, owing to the significant changes in the

Atmospheric
Chemistry
and Physics

Discussions

126 pollution sources, the physical and chemical characteristics of aerosols in NCP have
127 also changed evidently in recent years. Above all, the research on aerosol
128 hygroscopicity is still not enough for NCP. Further study is required, especially in the
129 area of f(RH). In this study, an improved high-resolution humidified nephelometer
130 system was used to observe the f(RH) of PM$_{2.5}$ for a wide RH range between 30%-96%
131 in the urban area of Beijing over three seasons (winter, summer, and autumn). The main
132 objectives of this article are to characterize the variations of f(RH) and other optical
133 parameters under different seasons and different pollution levels, and set up the optimal
134 expressions of f(RH).

135 **2. Instruments and methods**

136 **2.1 Observation site**

137   The measurement campaign was performed at the Institute of Urban Meteorological
138 in the Haidian district (about 36m above the ground), which located in the northwest
139 urban area of Beijing, outside the third-ring road (39°56'N, 116°17'E). The sampling
140 site was located next to a high-density residential area, which has no significant
141 emissions from industrial in the surrounding neighborhood. Therefore, the observation
142 data could represent the air quality levels of the typical urban area of Beijing. The
143 observations were conducted in three seasons, 12nd Jan. to 14th Feb. for winter, 6th Jul.
144 to 21st Aug. for summer, and 30th Sep. to 13th Nov. for autumn.

145 **2.2 Instruments**

146   The f(RH) was measured by a dual-nephelometer system, one nephelometer for the
147 aerosol scattering coefficient under dry condition, and another nephelometer for the
148 humidified aerosol. The air flow first passed through a PM$_{2.5}$ inlet, and then was dried
149 by two tandem Nafion dryers (MD-700), which could reduce the RH of air flow lower
150 than 30%. The dried air was separated into two paths, one stream went directly into a
151 nephelometer, another stream was humidified by passing through a Gore-Tex tube,
152 which was set in a stainless steel tube. The interlayer between these two tubes is
153 circulating water headed by the water bath. The minutely scattering coefficients of dry
154 and humidified PM$_{2.5}$ under three wavelengths (450, 525, and 635nm) were
155 synchronously measured by these two nephelometers (Aurora 3000). In most studies,
156 there was only one water bath been used for humidifying. After a humidifying process,
157 it is necessary to wait for the water in the water bath to cool down enough for the next
158 process. Differently, in this study, two water baths were used. When one water bath was
159 heating up the water for humidifying, another water bath was cooling down the water
160 itself. After a humidifying process, the water bath with cool water would be switched
161 into the humidification pipeline. The use of two water baths could ensure that the
162 effective data of f(RH) is more than twice that of using only one water bath. The
163 temperature of water in the water bath was controlled by an automatic system to ensure
164 the humidifying effect.

165   Two combined RH and temperature sensors (Vaisala HMP110) were set at the inlet
166 and outlet of the wet nephelometer, respectively. The vapor pressures were calculated
167 by the sensor data, and the average value was considered as the vapor pressure in the
168 optical chamber. Thus, the humidified RH in the chamber could be calculated through
169 the derived vapor pressure and the temperature measured by the sensor in the chamber.

170   As mentioned above, the RH could not be accurately measured by a sensor when it is
171   above 90%. In order to accurately obtain higher relative humidity, the optical chamber
172   of wet nephelometer was deliberately cooled with the temperature lower than that at the
173   inlet and outlet. So the humidified RH could be higher than 95% in the chamber when
174   the RH at the inlet and outlet were lower than 90%. This method makes it possible to
175   observe the f(RH) under high RH. To avoid the vapor condensation and particle
176   activation, the upper limit of humidified RH in the optical chamber of wet nephelometer
177   was set to 97%, which made the effective data of f(RH) could reach RH of 96%. Each
178   humidifying process lasted about 50 minutes, and all the minutely average data were
179   automatically recorded by the control system. During the observation periods, these
180   two nephelometers were calibrated every ten days. Since two Vaisala sensors and two
181   nephelometers were all newly purchased and the relative error of vapor pressures was
182   always less than 1%, the sensors were not calibrated during the observation.

183   Other than the f(RH) measurement, the six-minute average $PM_{2.5}$ mass
184   concentrations were also measured by a continuous dichotomous ambient air monitor
185   (TEOM 1405DF). The sample filter and sample conditioner filter of this monitor were
186   replaced every 15 days or when the dust loading exceeded 70%. The five-minute
187   average absorption coefficient of $PM_{2.5}$ was monitored by a multiangle absorption
188   photometer (MAAP 5012). The quartz-fiber filter could be automatically changed when
189   the light transmission was less than 20%. In addition, the hourly water-soluble ions
190   (SO_4^{2-}, NO_3^-, Cl^-, NH_4^+, Na^+, K^+, Mg^{2+}, and Ca^{2+}) of $PM_{2.5}$ and trace gases (HCl, HNO_3,
191   HNO_2, SO_2, and NH_3) were measured by an online analyzer (MARGA). In addition,
192   the aerosol number concentration distribution (SMPS3938+APS3321), and size-
193   resolved chemical compositions (MOUDI 122) were also synchronously measured
194   during these three observation periods.

195   In this paper, we mainly focus on the discussions of f(RH). In the near future, the
196   aerosol hygroscopicity would be comprehensively evaluated by making a use of all the
197   results from the above-mentioned observations and would be published in the following
198   papers.

199   **2.3 Methods**

200   The scattering Ångström exponent (Ångström, 1930) between 450 and 635nm ($Å_{450-}$
201    $_{635}$) at dry condition (RH<30%) characterizes the wavelength dependence of aerosol
202   scattering coefficients and was calculated using the scattering coefficient at
203   wavelengths of 635 and 450 nm by the following equation:

204    $$Å_{450-635} = (\log \sigma_{sp}(450) - \log \sigma_{sp}(635) / (\log 635 - \log 450) \tag{1}$$

205   The $PM_{2.5}$ absorption coefficient was measured in the wavelength of 670nm by MAAP.
206   In order to facilitate comparison, we transform the absorption coefficient of 670nm into
207   that of 525nm according to the assumption that absorption is inversely proportional to
208   wavelength (Bond and Bergstrom, 2006; Liu et al., 2018). Thus, the SSA at 525nm
209   (SSA_{525nm}) was the proportion of the scattering coefficient to the sum of scattering
210   coefficient and absorption coefficient.

211   When the air is very clean, the relative change and fluctuation of the particle
212   concentration in the ambient air would be more intense. Furerthmore, the airflow into
213   two nephelometers could not be completely synchronized during the observation. The

Atmospheric
Chemistry
and Physics
Discussions

214 larger relative error of scattering coefficient in two nephelometers could lead to greater
215 fluctuations in f(RH) during the humidifying cycle when under clean conditions
216 because the f(RH) is the ratio of the scattering coefficients from humidified and dry
217 nephelometers. Thus, the f(RH) points with dry scattering coefficient at 525nm less than
218 50 were removed from the fitting of the f(RH) curves. In this paper, the f(RH)
219 discussions are all based on the data of 525nm if not specifically pointed out.

220   The $PM_{2.5}$ concentrations are classified into three groups with 0~35 μg m^{-3}, 35~75
221 μg m^{-3}, and >75 μg m^{-3}, representing very clean, moderately clean, and polluted
222 conditions referring to the AQI grading standard of China, respectively. The reason for
223 this division is mainly based on the characteristics of f(RH) data.

3. Results and discussions

3.1 Overview of the optical properties and f(RH) of $PM_{2.5}$

226   Fig. 1 shows an overview of the hourly averaged light scattering coefficients
227 ($\sigma_{sca,525nm}$), absorption coefficients ($\sigma_{ap,630nm}$), single scattering albedo (SSA_{630nm}), and
228 scattering Ångström exponent ($\mathring{A}_{450-635}$) as well as f(RH) at RH=80% (f(80%)) for $PM_{2.5}$.
229 The average values of optical parameters and f(80%) in different seasons and under
230 different $PM_{2.5}$ pollution levels are listed in Table 1.

231   The $PM_{2.5}$ pollution was heaviest in the winter observation period and lightest in
232 summer. The scattering coefficient and absorption coefficient also show the same trends.
233 Single scattering albedo is one of the most important parameters in estimating of the
234 direct aerosol radiative forcing. The SSA_{525} increased with the aggravation of $PM_{2.5}$
235 pollution in all three seasons, indicating that the components with strong scattering
236 ability, such as secondary ions, increased significantly during the pollution process. The
237 wind rose of SSA_{525} in Figure 2 also indicates that the higher SSA_{525} values generally
238 occurred under the southerly wind condition which was often accompanied by higher
239 $PM_{2.5}$ concentrations.

240   Scattering Ångström exponent is generally regarded as an indicator of particle size.
241 In winter, lower $\mathring{A}_{450-635}$ was observed in less polluted conditions. As depicted in Figure
242 2, the clean conditions in winter occurred mainly in the case of northwest wind with
243 relatively higher wind speed, which led to a greater proportion of larger particles such
244 as crustal dust in the air. Conversely, the $\mathring{A}_{450-635}$ in polluted condition was lowest in
245 summer. Compared with winter, the relative humidity in summer was much higher,
246 especially under the condition of pollution, which could make particle collision and
247 coagulation easier to occur Guo et al (2014).

248   According to the ZSR (Zdanovskii-Stokes-Robinson) assumption (Zdanovskii, 1948;
249 Stokes and Robinson, 1966), the κ value of a multicomponent particle is equal to the
250 volume weighted average of each component. As depicted in Figure 1, the f(80%) at
251 525nm is highly correlated with the fractions of all the water-soluble ions to $PM_{2.5}$.
252 Owing to the proportion of hygroscopic components increased, $PM_{2.5}$ had higher f(80%)
253 in the polluted conditions. The standard deviations (SD) of f(80%) also indicate that the
254 changes of fractions of hygroscopic components were relatively small when the $PM_{2.5}$
255 over 35μg m^{-3} in summer and autumn. The wind roses obviously reveal the differences
256 in the hygroscopicity and chemical compositions of $PM_{2.5}$ from different directions.
257 The f(80%) values in this study are in agreement with the range of values reported in

Atmospheric
Chemistry
and Physics
Discussions

Open Access

258   some other studies of the North China Plain (Table 2). Overall, the diurnal variation of
259   $f(80)$ is not obvious, and the average $f(80)$ at 12 to 16 pm was slightly higher (Figure
260   3).

261

262   **Table 1**

263

264   **Table 2**

265

266   **Figure 1**

267

268   **Figure 2**

269

270   **Figure 3**

271

3.2 Parameterization schemes of $f(RH)$

273   To better describe the dependence of $f(RH)$ on RH, many different empirical
274   expressions have been applied in previous studies to fit the $f(RH)$ measurements.
275   Kotchenruther et al. (1999) proposed that different fitting equations should be used
276   according to the observed curve structure. For monotonic curves in which $f(RH)$ varies
277   smoothly with RH, they proposed the use of equation reported by Kasten (1969) and its
278   variants. The most commonly used equation is the one-parameter fit equation (Hänel,
279   1980; Gassó et al., 2000; Brock et al. 2016) and (Kotchenruther and Hobbs, 1998;
280   Carrico et al., 2003; Zieger et al., 2011; Chen et al., 2014). For deliquescent curves,
281   Kotchenruther et al. (1999) introduced a more complex equation, and more detailed
282   information and fitting equations could be found in Titos et al. (2016).

283   In this work, four commonly used empirical parameterization schemes were chosen
284   to describe the monotonic curves of $f(RH)$ variation:

285         $f(RH)=a\,(1-RH/100)^{-\gamma(RH/100)}$ Chen et al. (2014)   (2)
286         $f(RH)=a\,(1-RH/100)^{-\gamma}$ Kasten (1969)   (3)
287         $f(RH)=1+a\,(RH/100)^{\gamma}$ Kotchenruther and Hobbs, (1998)   (4)
288         $f(RH)=1+a\,(RH/(100-RH))$ Brock et al. (2016)   (5)
289   where γ parameterizes the magnitude of the scattering enhancement, which is not
290   affected by the RH. The comparison of the fitting results for different expressions is
291   shown in figure S1 to S3. According to the fitting results, R^2, and the comparison
292   between fitting $f(80\%)$ values and measured ones, we finally choose the Eq. (2) to
293   describe the scattering enhancement due to monotonic hygroscopic growth.

294

295   **Figure 4**

296

297   **Figure 5**

298

299   **Figure 6**

300

301   **Table 3**

Atmospheric
Chemistry
and Physics
Discussions

302
303   In our previous studies, the pollution of particulate matter was usually classified into
304   three categories through two threshold values of PM$_{2.5}$ concentrations, 75μg·m^{-3} and
305   150μg·m^{-3}, for clean, moderately polluted, and heavily polluted conditions. In this study,
306   we found that the scatter points of f(RH) were quite concentrated near the fitting curves
307   when the PM$_{2.5}$ was above 75μg·m^{-3}, and the fitting parameters were markedly different
308   for conditions of PM$_{2.5}$ above and under 35μg·m^{-3}. Consequently, we use 35μg·m^{-3} and
309   75μg·m^{-3} as boundaries to classify the different pollution levels in this study. Fig. (4) to
310   Fig. (6) show the fitting f(RH) curves under very clean, moderately clean, and polluted
311   conditions for three seasons. Table 3 shows the fitting results from this work and a
312   previous study conducted in NCP, which used the same equation expression (Chen et
313   al., 2014). Except for the very clean condition in winter, the fitting values of a are all
314   near 1.0 and the fitting f(RH) curves are all above 1.0 for RH above 30%. However, the
315   fitting f(RH) curve shown in Fig 4a is apparently under the observed data points and
316   lower than 1.0 when RH under 40%. It means that the fitting curve of the very clean
317   condition in winter would underestimate the f(RH) value when RH is below 40%. It
318   can be seen from Figure 5 and Figure 6 that the fitting R^2 increases and the points
319   become more concentrated along with the aggravation of PM$_{2.5}$ pollution in summer
320   and autumn. This is in accordance with the characteristics of the SD of f(80) in Figure
321   3. Differently, the f(RH) points are still dispersed even under the polluted condition of
322   winter. This indicates that the chemical compositions of PM$_{2.5}$ when under the condition
323   of pollution were more stable in summer and autumn.
324   By comparing the fitting curves of different seasons and different pollution
325   conditions, it is found that the f(RH) curve of the very clean condition is lower than that
326   of other two pollution levels for each season. Except for the very clean condition in
327   winter and autumn, the fitting curves for the other seven conditions are relatively close,
328   especially when RH less than 90%. In the study of Chen et al. (2014), a segment fitting
329   with the critical RH of 60% is applied in the parameterization of f(RH). Comparing the
330   fitting results in Table 3, we find that the f(RH) values with RH above 80% from fitting
331   curves for clean and polluted conditions in Chen's study are evidently lower than those
332   from the respective curves for very clean and polluted conditions in this work. It
333   indicates that the scattering enhancement due to moisture uptake or hygroscopicity of
334   aerosol under high RH is probably higher than before.
335   In addition, the averaged f(RH) at 450nm, 525nm, and 635nm was also fitted
336   separately for each season. It is clear that the f(RH) showed a dependence on
337   wavelength, especially in summer. The averaged f(RH) increased with increasing
338   wavelength. Similar results were also obtained by Zhang et al. (2015) at Lin'an, China
339   and Zieger et al. (2014) at a regional continental research site in Melpitz, Germany.
340   However, we found that when under very clean conditions in winter and autumn, the
341   mean value of f(80) at 450nm was higher than that at 525nm and 635nm (Fig. S4), and
342   it is more obvious in winter. Through further curve fitting of f(RH) at different
343   wavelengths for three seasons, it is also found that the f(RH) curve of 450nm was
344   evidently higher than that of 525nm and 635nm only under very clean conditions in
345   winter. Our previous work showed that the sulfates, nitrates, and ammonium (SNA)

Atmospheric
Chemistry
and Physics
Discussions

346 were abundant in aerodynamic diameter of 0.18~1.0μm on clean days in winter with
347 the mass median diameters (MMD) of SNA at about 0.45μm. However, the SNA was
348 mainly concentrated in 0.32~1.8μm with evidently higher MMDs on polluted days or
349 in other seasons (Zhao et al., 2017; Su et al., 2018). The high fraction of SNA in
350 particles below 500 nm might be responsible for the higher f(RH) at 450nm when under
351 very clean conditions in winter.

352 **3.3 Uncertainty analysis for f(RH) measurements**

353 As mentioned above, the humidified RH in the wet nephelometer was calculated
354 through the derived average vapor pressure and the temperature measured by the sensor
355 in the chamber. According to the differences in vapor pressure values from the sensors
356 at the inlet and outlet, a relative error of 0.5% could be calculated for the vapor pressure
357 data. And the mean absolute error of the temperature measurement in the nephelometer
358 was 0.2℃. Then, a Monte Carlo simulation was utilized to estimate the uncertainty of
359 calculated humidified RH values. New values of vapor pressure and temperature were
360 simulated by adding the uncertainties of 0.5% and 0.2℃ to the observation data
361 (following a normal distribution). And new humidified RH could be calculated using
362 the simulated data, and this procedure was repeated 1000 times for each humidified RH
363 value. Then the average standard error of humidified RH in the wet nephelometer could
364 be calculated to be 0.85%.

365 Next, the Monte Carlo simulation was used again. The RH was assumed to range
366 from 20% to 90% with steps of 1**,** and assuming that γ ranges from 0 to 1 with steps of
367 0.01. The chosen interval for γ covers the particle types from non-hygroscopic aerosol
368 particles to very hygroscopic particles. Therefore, more than 7000 conditions were
369 simulated, and each condition corresponded to one set of RH and γ. For each condition,
370 the dry scattering coefficients with a wide range of 1 to 1000 Mm^{-1} were selected 5000
371 times as random numbers to present different atmospheric situations and aerosol loads.
372 The wet scattering coefficients were calculated associated with the previously selected
373 dry scattering coefficient and the f(RH) calculated by Eq. (2). A random error
374 (following a normal distribution with a standard variation of 0.85%) was also added to
375 the RH and the parameter a was set 1.0 when calculating the f(RH). According to the
376 manual of nephelometer Aurora 3000, the standard error of aerosol scattering
377 coefficient is 2.5%. Then we simulated the dry and wet scattering coefficients by
378 assuming that they both had an uncertainty of 2.5% (following a normal distribution).
379 Thus, the simulated f(RH) can be calculated again.

380 The mean and relative standard deviation of simulated f(RH) were calculated for each
381 RH and γ and are shown in Fig. 7. For aerosols in this work (γ ~ 0.35), f(RH) errors
382 were below 4% with RH lower than 85% while reached 9.7% when RH= 96%, which
383 can be regarded as a conservative estimation. And other unpredictable factors
384 contributing to f(RH) uncertainty have not been considered in this approach.

Figure 7

387 **4. Conclusions**

388 A wide-range (30%-96%) and high-resolution humidified nephelometer system was
389 developed and a measurement campaign was conducted to study the f(RH) for three

Atmospheric
Chemistry
and Physics
Discussions
Open Access
EGU

390 seasons in 2017. The f(RH) at higher RH had firstly been monitored and reported.

391 Based on the overview of the optical properties and f(RH) of PM$_{2.5}$, we found that
392 the higher SSA$_{525}$ values generally occurred under the southerly wind components with
393 higher PM$_{2.5}$ concentrations. The f(80%) at 525nm of PM$_{2.5}$ was evidently higher under
394 the polluted conditions and highly correlated with the fractions of all the water-soluble
395 ions. The average f(80) at 12 to 16 pm was slightly higher than that of other periods
396 from the average diurnal variations.

397 By comparing the fitting results and curves of four different empirical
398 parameterization schemes, it was found that one of the two-parameter fit equations can
399 better fit the observed f(RH) data. The fitting curves could be widely applied to the
400 studies of atmospheric visibility, radiative force, or liquid water content due to aerosol
401 moisture absorption. For summer and autumn, the f(RH) points of polluted conditions
402 were more concentrated near the fitting curves in the scatter plots with higher fitting R^2.
403 And the fitting curve under the very clean condition was lower than that of other
404 conditions for each season. Compared with the fitting curves in the previous study, the
405 hygroscopicity of aerosol under higher RH has probably been enhanced. In summer,
406 the fitting f(RH) showed a significant dependence on wavelength and increased with
407 increasing wavelength for each pollution condition. Nevertheless, the f(RH) curve of
408 450nm was evidently higher than that of 525nm and 635nm under the very clean
409 condition in winter, due to the higher fraction of SNA in particles below 500 nm.

410 The uncertainties of f(RH) were simulated by considering all the predictable
411 uncertainties or errors during the measurement, which was below 10% for RH up to
412 96%.

413

414 *Data availability.* All data in this work are available by contacting the corresponding
415 author P. S. Zhao (pszhao@ium.cn).

416

417 *Author contributions.* P Z designed and performed this study. P Z and J D analyzed the
418 data and discussed the results. P Z prepared the manuscript and J D prepared all the
419 figures. X D and J S calibrated the device and collected the data.

420

421 *Competing interests.* The authors declare that they have no conflict of interest.

422

429

References

431 Albrecht, B. A.: Aerosols, cloud microphysics, and fractional cloudiness, Science, 245, 1227-1230,
432   1989.
433 Brock, C. A., Wagner, N. L., Anderson, B. E., Attwood, A. R., Beyersdorf, A., Campuzano-Jost, P.,

434   Carlton, A. G., Day, D. A., Diskin, G. S., Gordon, T. D., Jimenez, J. L., Lack, D. A., Liao, J.,
435   Markovic, M. Z., Middlebrook, A. M., Ng, N. L., Perring, A. E., Richardson, M. S., Schwarz, J.
436   P., Washenfelder, R. A., Welti, A., Xu, L., Ziemba, L. D., and Murphy, D. M.: Aerosol optical
437   properties in the southeastern United States in summer – Part 1: Hygroscopic growth, Atmos.
438   Chem. Phys., 16, 4987-5007, 2016.
439   Carrico, C. M., Kus, P., Rood, M. J., Quinn, P. K., and Bates, T. S.: Mixtures of pollution, dust, sea
440   salt, and volcanic aerosol during ACE-Asia: Radiative properties as a function of relative
441   humidity, J. Geophys. Res., 108(D23), 8650, doi:10.1029/2003JD003405, 2003.
442   Carrico, C., Rood, M., Ogren, J., Neusüß, C., Wiedensohler, A., and Heintzenberg, J.: Aerosol
443   optical properties at Sagres, Portugal, during ACE-2, Tellus B, 52, 694–715, 2000.
444   Charlson, R. J., Schwartz, S. E., Hales, J. M., Cess, R. D., Coakley, J. A., Jr., Hansen, J. E., and
445   Hofmann, D. J.: Climate forcing by anthropogenic aerosols, Science, 255, 423-430, 1992.
446   Chen, J., Zhao, C. S., Ma, N., Liu, P. F., Göbel, T., Hallbauer, E., Deng, Z. Z., Ran, L., Xu, W. Y.,
447   Liang, Z., Liu, H. J., Yan, P., Zhou, X. J., and Wiedensohler, A.: A parameterization of low
448   visibilities for hazy days in the North China Plain, Atmos. Chem. Phys., 12, 4935-4950, 2012.
449   Chen, J., Zhao, C. S., Ma, N., and Yan, P.: Aerosol hygroscopicity parameter derived from the light
450   scattering enhancement factor measurements in the North China Plain, Atmos. Chem. Phys., 14,
451   3459–3497, 2014.
452   Chen, Y. N., Zhao, P. S., He, D., Dong, F., Zhao, X. J., and Zhang X. L.: Characteristics and
453   parameterization for atmospheric extinction coefficient in Beijing (In Chinses), Environ. Sci.,
454   36, 3582-3589, 2015.
455   Cheng, Y. F., Wiedensohler, A., Eichler, H., Heintzenberg, J., Tesche, M., Ansmann, A., Wendisch,
456   M., Su, H., Althausen, D., Herrmann, H., Gnauk, T., Brüggemann, E., Hu, M., and Zhang, Y. H.:
457   Relative humidity dependence of aerosol optical properties and direct radiative forcing in the
458   surface boundary layer at Xinken in Pearl River Delta of China: An observation based numerical
459   study, Atmos. Environ., 42, 6373–6397, 2008.
460   Cheng, Y. F, Zheng, G. J., Wei, C., Mu, Q., Zheng, B., Wang, Z. B., Gao, M., Zhang, Q., He, K. B.,
461   Carmichael, G., Pöschl, U., and Su, H.: Reactive nitrogen chemistry in aerosol water as a source
462   of sulfate during haze events in China, Sci. Adv., 2, e1601530, doi:10.1126/sciadv.1601530,
463   2016.
464   Covert, D. S., Charlson, R. J., and Ahlquist, N. C.: A study of the relationship of chemical
465   composition and humidity to light scattering by aerosol, J. Appl. Meteorol., 11, 968-976, 1972.
466   Day, D. E., Malm, W. C., and Kreidenweis, S. M.: Aerosol light scattering measurements as a
467   function of relative humidity, J. Air & Waste Manag. Assoc., 50, 710-716. 2000.
468   DeBell, L. J., Gebhart, K. A., Hand, J. L., Malm, W. C., Pitchford, M. L., Schichtel, B. A., and White,
469   W. H.: Spatial and seasonal patterns and temporal variability of haze and its constituents in the
470   United States-Report IV, Cooperative Institute for Research in the Atmosphere, Colorado State
471   University, 2006.
472   Fierz-Schmidhauser, R., Zieger, P., Gysel, M., Kammermann, L., DeCarlo, P. F., Baltensperger, U.,
473   and Weingartner, E.: Measured and predicted aerosol light scattering enhancement factors at the
474   high alpine site Jungfraujoch, Atmos. Chem. Phys., 10, 2319-2333, 2010.
475   Fierz-Schmidhauser, R., Zieger, P., Wehrle, G., Jefferson, A., Ogren, J. A., Baltensperger, U., and
476   Weingartner, E.: Measurement of relative humidity dependent light scattering of aerosols, Atmos.
477   Meas. Tech., 3, 39-50, 2010.

478 Gassó, S., Hegg, D. A., Covert, D. S., Collins, D., Noone, K. J., Öström, E., Schmid, B., Russell, P.
479   B., Livingston, J. M., Durkee, P. A., and Jonsson, H.: Influence of humidity on the aerosol
480   scattering coefficient and its effect on the upwelling radiance during ACE-2, Tellus B, 546-567,
481   2000.
482 Guo, S., Hu, M., Zamorab, M. L., Peng, J. F., Shang, D. J., Zheng, J., Du, Z. F., Wu, Z. J., Shao, M.,
483   Zeng, L. M., Molinac, M. J., and Zhang, R. Y.: Elucidating severe urban haze formation in China,
484   Proc. Natl. Acad. Sci. U S A, doi:10.1073/pnas.1419604111, 2014.
485 Hänel, G.: Technical Note: an attempt to interpret the humidity dependencies of the aerosol
486   extinction and scattering coefficients, Atmos. Environ., 15, 403-406, 1980.
487 Hinds, W. C.: Physical and chemical processes in aerosol system, in: Kulkarni P, Baron P A, and
488   Willeke K (Eds.): Aerosol Measurement: Principles, Techniques, and Applications, 3rd edition,
489   John Wiley & Sons, Inc, Hoboken, 41-54, 2011.
490 Jang, M., Czoschke, N.M., Lee, S., and Kamens, R.M.: Heterogeneous atmospheric aerosol
491   production by acid-catalyzed particle-phase reactions, Science, 298, 814-817, 2002.
492 Kasten, F.: Visibility forecast in the phase of pre-condensation, Tellus, 21, 631-635, 1969.
493 Köhler, H.: The nucleus in and the growth of hygroscopic droplets, Trans. Faraday. Soc., 32, 1152–
494   1161, 1936.
495 Kolb, C. E., Cox, R. A., Abbatt, J. P. D., Ammann, M., Davis, E. J., Donaldson, D. J., Garrett, B. C.,
496   George, C., Griffiths, P. T., Hanson, D.R., Kulmala, M., McFiggans, G., Pöschl, U., Riipinen, I.,
497   Rossi, M.J., Rudich, Y., Wagner, P. E., Winkler, P. M.,Worsnop, D. R., and O'Dowd, C. D.: An
498   overview of current issues in the uptake of atmospheric trace gases by aerosols and clouds,
499   Atmos. Chem. Phys., 10, 10561-10605, 2010.
500 Koloutsou-Vakakis, S., Carrico, C. M., Kus, P., Rood, M. J., Li, Z., Shrestha, R., Ogren, J. A., Chow,
501   J. C., and Watson, J. G.: Aerosol properties at a midlatitude Northern Hemisphere continental
502   site, J. Geophys. Res., 106 (D3), 3019-3032, 2001.
503 Kotchenruther, R. A., Hobbs, P. V., and Hegg, D. A.: Humidification factors for atmospheric aerosols
504   off the mid-Atlantic coast of the United States, J. Geophys. Res., 104 (D2), 2239–2251, 1999.
505 Kotchenruther, R. A., and Hobbs, P. V.: Humidification factors of aerosols from biomass burning in
506   Brazil, J. Geophys. Res., 103, 32081-32089, 1998.
507 Kuang, Y., Zhao, C. S., Tao, J. C., Bian, Y. X., Ma, N., and Zhao, G.: A novel method for deriving
508   the aerosol hygroscopicity parameter based only on measurements from a humidified
509   nephelometer system, Atmos. Chem. Phys., 17, 6651-6662, 2017.
510 Kuang, Y., Zhao, C. S., Zhao, G., Tao, J. C., Xu, W., Ma, N., and Bian, Y. X.: A novel method for
511   calculating ambient aerosol liquid water content based on measurements of a humidified
512   nephelometer system, Atmos. Meas. Tech., 11, 2967-2982, 2018.
513 Liu, B. Y. H., Pui, D. Y. H., Whitby, K. T., Kittelson, D. B., Kousaka, Y., and McKenzie, R.L.: The
514   aerosol mobility chromatograph: A new detector for sulfuric-acid aerosols, Atmos. Environ., 12,
515   99-104, 1978.
516 Liu, C., Chung, C. E., Yin, Y., and Schnaiter, M.: The absorption Ångström exponent of black carbon:
517   from numerical aspects, Atmos. Chem. Phys., 18, 6259-6273, 2018.
518 Liu, H. J.: Measurement of aerosol light scattering enhancement factor and study on hygroscopicity
519   parameter, Ph.D. thesis, Peking University, Beijing, China, 2015.
520 Liu, H. J., and Zhao, C. S.: Design of a humidified nephelometer system with high time resolution
521   (in Chinese), Acta Sci. Natur. Univ. Pekin., 52, 999-1004. 2016.

Atmospheric
Chemistry
and Physics
Discussions

522   Liu, P. F., Zhao, C. S., Gobel, T., et al.: Hygroscopic properties of aerosol particles at high relative
523   humidity and their diurnal variations in the North China Plain, Atmos. Chem. Phys., 11, 3479-
524   3494, 2011.
525   Liu, Z., Wu, L.Y., Wang, T. H., and Wang, W.G.: Uptake of methacrolein into aqueous solutions of
526   sulfuric acid and hydrogen peroxide, J. Phys. Chem. A, 116, 437-442, 2012.
527   Massling, A., Stock, M., Wehner, B., Wu, Z. J., Hu, M., Brüggemann, E., Gnauk, T., Herrmann, H.,
528   and Wiedensohler, A.: Size segregated water uptake of the urban submicrometer aerosol in
529   Beijing, Atmos. Environ., 43, 1578–1589, 2009.
530   McMurry, P. H. and Wilson, J.C.: Droplet phase (Heterogeneous) and gas phase (homogeneous)
531   contributions to secondary ambient aerosol formation as functions of relative humidity, J.
532   Geophys. Res., 88, 5101-5108, 1983.
533   Meier, J., Wehner, B., Massling, A., Birmili, W., Nowak, A., Gnauk, T., Brüggemann, E., Herrmann,
534   H., Min, H., Wiedensohler, A.: Hygroscopic growth of urban aerosol particles in Beijing (China)
535   during wintertime: a comparison of three experimental methods, Atmos. Chem. Phys., 9, 6865–
536   6880, 2009.
537   Pan, X. L., Yan, P., Tang, J., Ma, J. Z., Wang, Z. F., Gbaguidi, A., and Sun, Y. L.: Observational
538   study of influence of aerosol hygroscopic growth on scattering coefficient over rural area near
539   Beijing mega-city, Atmos. Chem. Phys., 9, 7519-7530, 2009.
540   Petters, M. D. and Kreidenweis, S. M.: A single parameter representation of hygroscopic growth
541   and cloud condensation nucleus activity, Atmos. Chem. Phys., 7, 1961-1971, 2007.
542   Pilat, M. J. and Charlson, R. J.: Theoretical and optical studies of humidity effects on the size
543   distribution of hygroscopic aerosol, J. Rech. Atmos.,1, 165-170, 1966.
544   Pitchord, M., Malm, W., Schichtel, B. Kumar, N., Lowenthal, D., and Hand, J.: Revised algorithm
545   for estimating light extinction from IMPROVE particle speciation data, J. Air & Waste Manag.
546   Assoc., 57, 1326-1336, 2007.
547   Ravishankara, A. R.: Heterogeneous and multiphase chemistry in the troposphere, Science, 276,
548   1058-1065, 1997.
549   Rood, M. J., Larson, T. V., Covert, D. S., and Ahlquist, N. C.: Measurement of laboratory and
550   ambient aerosols with temperature and humidity controlled nephelometry, Atmos. Environ., 19,
551   1181-1190, 1985.
552   Rosenfeld, D.: Suppression of rain and snow by urban and industrial air pollution, Science, 287,
553   1793-1796, 2000.
554   Schwartz, S. E., Arnold, F., Blanchet, J. P., Durkee, P. A., Hofmann, D. J., and Hoppel, W. A.: Group
555   report: connections between aerosol properties and forcing of climate, NJ: John Wiley, Hoboken,
556   251-80, 1995.
557   Seinfeld, J. H. and Pandis, S. N (Eds).: Atmospheric Chemistry and Physics: From Air Pollution to
558   Climate Change, 3rd edition, John Wiley & Sons, Inc, Hoboken, 325-361, 2016.
559   Stokes, R. H. and Robinson, R. A.: Interactions in aqueous nonelectrolyte solutions. I. Solute-
560   solvent equilibria, J. Phys. Chem., 70, 2126-2131, 1966.
561   Su, J., Zhao, P. S., and Chen, Y. N.: Chemical compositions and liquid water content of size-resolved
562   aerosol in Beijing, Aerosol Air Qual. Res., 18, 680-692, 2018.
563   Swietlicki, E., Hansson, H.C., Hämeri, K., Svenningsson, B., Massling, A., McFiggans, G.,
564   McMurry, P.H., Petäjä, T., Tunved, P., Gysel, M., Topping, D., Weingartner, E., Baltensperger,
565   U., Rissler, J., Wiedensohler, A., and Kulmala, M.: Hygroscopic properties of submicrometer

Atmospheric
Chemistry
and Physics
Discussions

566   atmospheric aerosol particles measured with H-TDMA instruments in various environments: a
567   review, Tellus B, 60, 432-469, 2008.

568 Tami, C. B., and Robert, W. B.: Light absorption by carbonaceous particles: an investigative review,
569   Aerosol Sci. Tech., 40, 27-67, 2006.

570 Tao, J. C, Zhao, C. S, Kuang, Y., Zhao, G., Shen, C. Y., Yu, Y. L., Bian, Y. X., and Xu, W. Y.: A new
571   method for calculating number concentrations of cloud condensation nuclei based on
572   measurements of a three-wavelength humidified nephelometer system, Atmos. Meas. Tech., 11,
573   895-906, 2018.

574 Titos, G., Cazorla, A., Zieger, P., Andrews, E., Lyamani, H., Granados-Muñoz, M. J., Olmo, F. J.,
575   Alados-Arboledas, L.: Effect of hygroscopic growth on the aerosol light-scattering coefficient:
576   A review of measurements, techniques and error sources, Atmos. Environ., 141, 494-507, 2016.

577 Twomey, S.: Pollution and the planetary albedo, Atmos. Environ., 8, 1251-1256, 1974.

578 Wang, J. and Martin, S. T.: Satellite characterization of urban aerosols: Importance of including
579   hygroscopicity and mixing state in the retrieval algorithms, J. Geophys. Res., 112, D17203,
580   doi:10.1029/2006JD008078, 2007.

581 Wang, Y., Wu, Z. J., Ma, N., Wu, Y. S., Zeng, L. M., Zhao, C. S., Wiedensohler, A.: Statistical
582   analysis and parameterization of the hygroscopic growth of the sub-micrometer urban
583   background aerosol in Beijing, Atmos. Environ., 175, 184-191, 2018.

584 Yan, P., Pan, X. L., Tang, J., et al.: Hygroscopic growth of aerosol scattering coefficient: A
585   comparative analysis between urban and suburban sites at winter in Beijing, Particuology, 7, 52-
586   60, 2009.

587 Zdanovskii, A. B.: New methods for calculating solubilities of electrolytes in multicomponent
588   systems, Zh. Fiz. Khim., 22, 1475-1485, 1948.

589 Zhang, L., Sun, J. Y., Shen, X. J., Zhang, Y. M., Che, H. C., Ma, Q. L., Zhang, Y. W., Zhang, X. Y.,
590   Ogren, J. A.: Observations of relative humidity effects on aerosol light scattering in the Yangtze
591   River Delta of China, Atmos. Chem. Phys., 15, 8439-8454, 2015.

592 Zhao, P. S., Chen, Y. N., and Su, J.: Size-resolved carbonaceous components and water soluble ions
593   measurement of ambient aerosol in Beijing, J. Environ. Sci., 54, 298-313, 2017.

594 Zieger, P., Fierz-Schmidhauser, R., Poulain, L., Müller, T., Birmili, W., Spindler, G., Wiedensohler,
595   A., Baltensperger, U., and Weingartner, E.: Influence of water uptake on the aerosol particle light
596   scattering coefficients of the Central European aerosol, Tellus B, 66, 22716, 2014.

597 Zieger, P., Kienast-Sjögren, E., Starace, M., von Bismarck, J., Bukowiecki, N., Baltensperger, U.,
598   Wienhold, F.G., Peter, T., Ruhtz, T., Collaud Coen, M., Vuilleumier, L., Maier, O., Emili, E.,
599   Popp, C., and Weingartner, E.: Spatial variation of aerosol optical properties around the high-
600   alpine site Jungfraujoch (3580 m a.s.l.), Atmos. Chem. Phys., 12, 7231-7249, 2012.

601 Zieger, P., Weingartner, E., Henzing, J., Moerman, M., de Leeuw, G., Mikkilä, J., Ehn, M., Petäjä,
602   T., Clémer, K., van Roozendael, M., Yilmaz, S., Frieβ, U., Irie, H., Wagner, T., Shaiganfar, R.,
603   Beirle, W., Apituley, A., Wilson, K., Baltensperger, U.: Comparison of ambient aerosol
604   extinction coefficients obtained from in-situ, MAX-DOAS and LIDAR measurements at
605   Cabauw. Atmos. Chem. Phys., 11, 2603-2624, 2011.

606

Table captions:

607

608　Table .1 Average $\sigma_{sca,525nm}$(dry), $\sigma_{abs,525nm}$(dry), SSA_{525}(dry), $Å_{450-635}$(dry), and f(80%)

609　under different pollution levels in three seasons.

610　Table 2. Comparisons of average f(80%) in different campaigns of NCP area.

611　Table 3. Comparisons of fitting parameters with another study using the same scheme.

612

613

614

Atmospheric
Chemistry
and Physics
Discussions

Open Access

615
616

Table 1

| | | Entire observation periods | PM$_{2.5}$ pollution levels (μg m^{-3}) | | |
			Very clean (PM$_{2.5}\leq$35)	Moderately clean (35 <PM$_{2.5}\leq$75)	Polluted (PM$_{2.5}$>75)
Winter	$\sigma_{sca,525nm}$(dry)	287±359	35±19	205±69	504±158
	$\sigma_{abs,525nm}$(dry)	46±37	10±7	41±13	75±15
	SSA$_{525}$(dry)	0.82±0.06	0.79±0.04	0.83±0.03	0.87±0.02
	Å$_{450-635}$(dry)	1.27±0.20	1.18±0.13	1.42±0.15	1.45±0.15
	f(80%)	1.47±0.16	1.31±0.12	1.51±0.09	1.60±0.14
Summer	$\sigma_{sca,525nm}$(dry)	170±125	85±46	226±87	410±121
	$\sigma_{abs,525nm}$(dry)	27±13	20±10	30±11	40±12
	SSA$_{525}$(dry)	0.83±0.09	0.79±0.09	0.87±0.05	0.91±0.02
	Å$_{450-635}$ (dry)	1.34±0.23	1.42±0.22	1.30±0.22	1.18±0.21
	f(80%)	1.54±0.16	1.50±0.19	1.60±0.08	1.62±0.06
Autumn	$\sigma_{sca,525nm}$(dry)	261±243	57±54	241±62	564±169
	$\sigma_{abs,525nm}$(dry)	38±24	17±12	40±16	61±18
	SSA$_{525}$(dry)	0.83±0.09	0.75±0.09	0.85±0.05	0.90±0.03
	Å$_{450-635}$(dry)	1.17±0.27	1.16±0.27	1.30±0.20	1.06±0.27
	f(80%)	1.53±0.11	1.44±0.14	1.58±0.08	1.57±0.04

617
618
619
620
621
622

Table 2

Study area (Campaign)	Periods	Aerosol pollution levels	f(RH=80%)	Wavelength (nm)	Reference
The rural site of Beijing	24 April–15 May 2006	Clean	1.31 ± 0.03	525	Pan et al. (2009)
		Urban pollution	1.57 ± 0.02		
		Special case	2.21		
SDZ, Beijing, a rural site	December 2005	Relatively clean	1.16	525	Yan et al. (2009)
		Relatively polluted	1.34		
CAMS, Beijing, an urban site		Relatively clean	1.2	525	
		Relatively polluted	1.48		
Wuqing, Tianjin	October 2009 to late January 2010	Clean	1.46 ± 0.15	550	Chen et al. (2014)
		Polluted	1.58 ± 0.19		
Wangdu, suburban district of North China Plain	4 June 2014 - 14 July 2014	Entire campaign	1.8 (1.1-2.3)	550	Kuang at al. (2017)
		deliquescent phenomena	2.0 (1.7-2.3)		

623
624

Atmospheric
Chemistry
and Physics
Discussions

Open Access

625

626   Table 3

	Periods		a	γ	Reference
Very clean			0.930	0.329	
Moderately clean	12 Jan.-14 Feb., 2017		0.971	0.372	
Polluted			0.988	0.356	
Very clean			0.972	0.355	
Moderately clean	6 July-21 Aug., 2017		0.980	0.362	This work
Polluted			0.984	0.371	
Very clean			0.979	0.334	
Moderately clean	30 Sep. to 13 Nov., 2017		1.002	0.344	
Polluted			1.014	0.332	
Entire campaign		RH<60%	1.02	0.21	
		RH≥60%	1.08	0.26	
Clean	Oct.2009-	RH<60%	1.00	0.10	Chen et al.
	Jan.2010	RH≥60%	1.00	0.26	(2014)
Polluted		RH<60%	1.03	0.26	
		RH≥60%	1.14	0.25	

627

628

Atmospheric
Chemistry
and Physics
Discussions

Open Access

EGU

Figure captions:

630 Figure 1. Time series of $\sigma_{sca,525nm}(dry)$, $\sigma_{abs,525nm}(dry)$, $SSA_{525}(dry)$, $Å_{450-635}(dry)$,

631 *f*(80%), and mass concentrations of water-soluble ions and their mass fractions over

632 all the sampling periods in three seasons.

633 Figure 2. Wind dependence of $\sigma_{sca,525nm}(dry)$, $\sigma_{abs,525nm}(dry)$, $SSA_{525}(dry)$, $Å_{450-635}(dry)$,

634 and *f*(80%) over three seasons; the shaded contour indicates the average of variables

635 for varying wind speeds and wind directions.

636 Figure 3. Diurnal variations of *f*(80%) in different seasons.

637 Figure 4. Fitting *f*(RH) curves under different pollution levels in winter.

638 Figure 5. Fitting *f*(RH) curves under different pollution levels in summer.

639 Figure 6. Fitting *f*(RH) curves under different pollution levels in autumn.

640 Figure 7. Simulated *f*(RH) and its error (color scale) as a function of RH and the

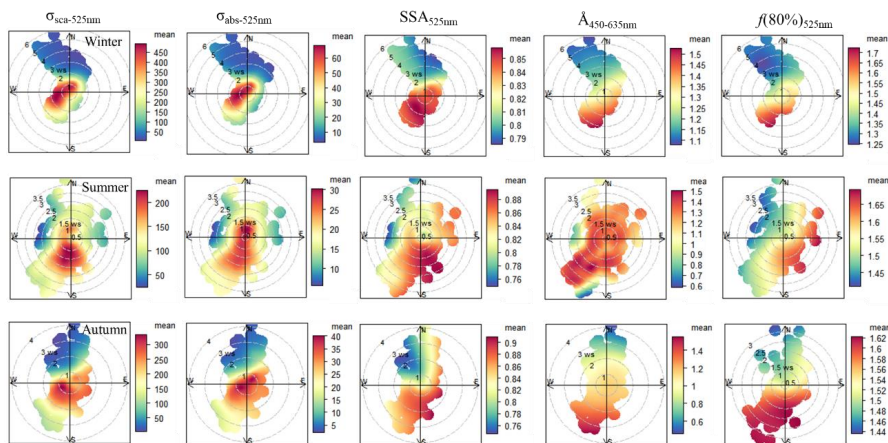641 hygroscopic parameter γ.

642

643

644

645

646

647
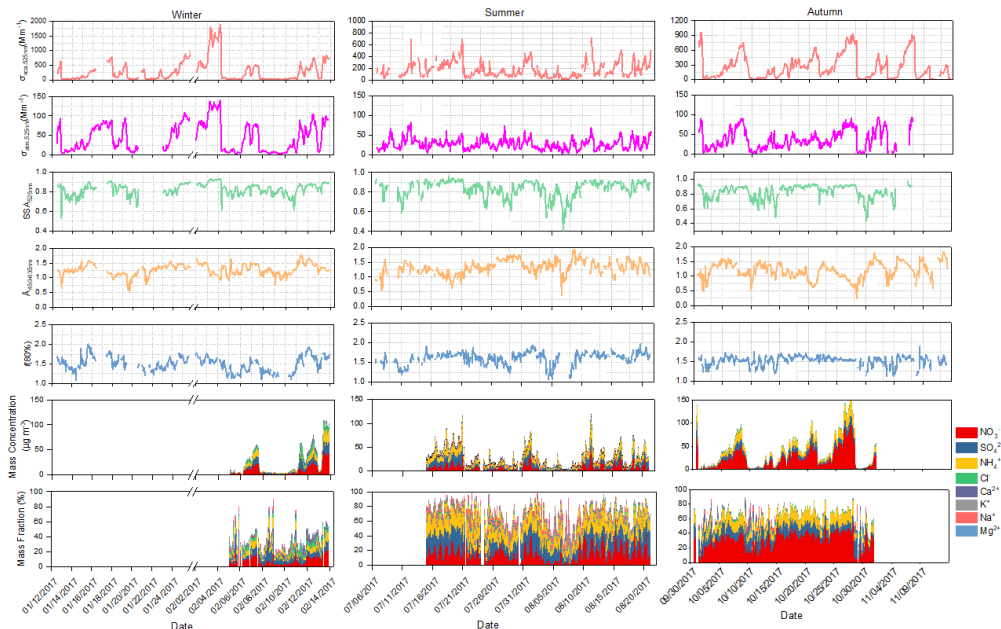
649   Figure 1

650

651

652

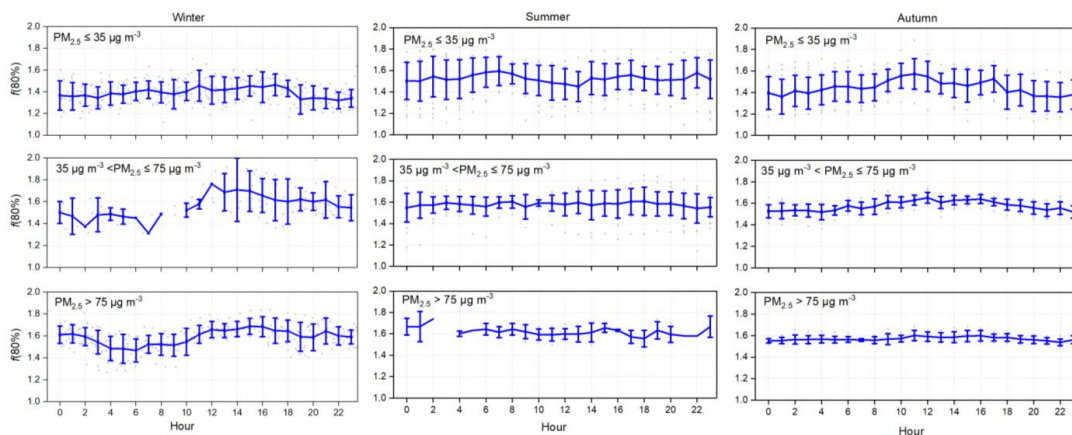

653

654   Figure 2

655
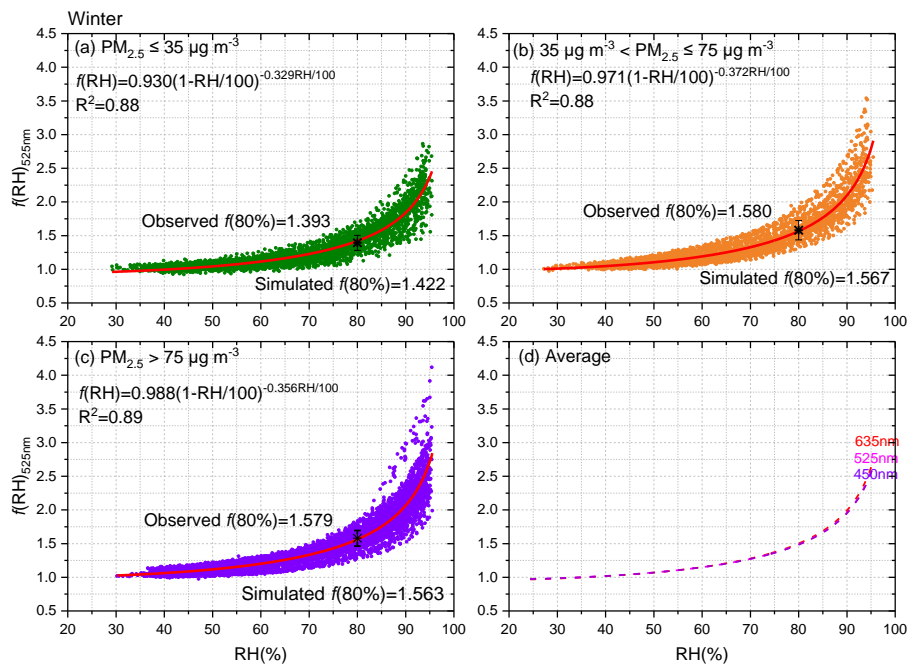
656

657

658

659

Atmospheric
Chemistry
and Physics
Discussions
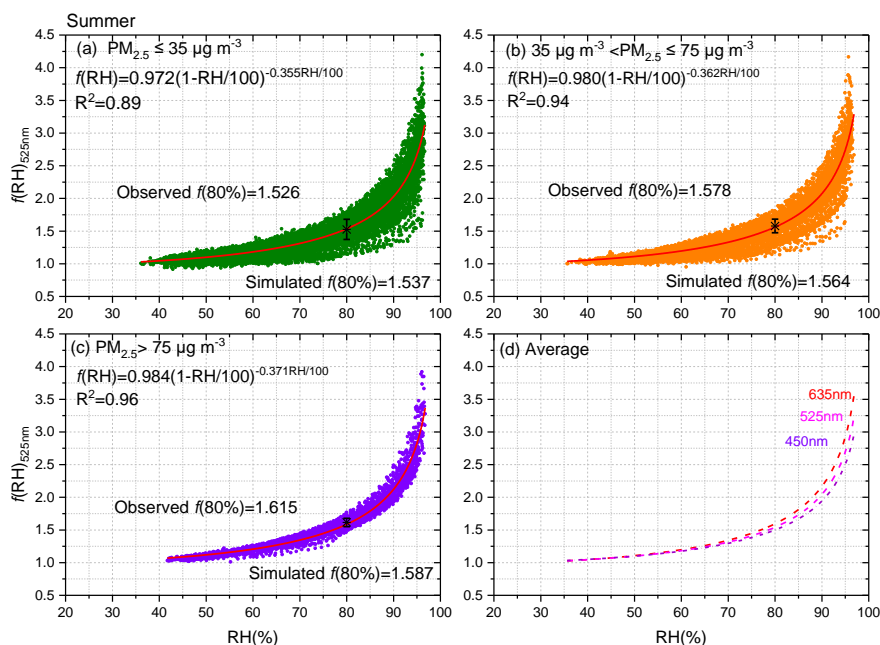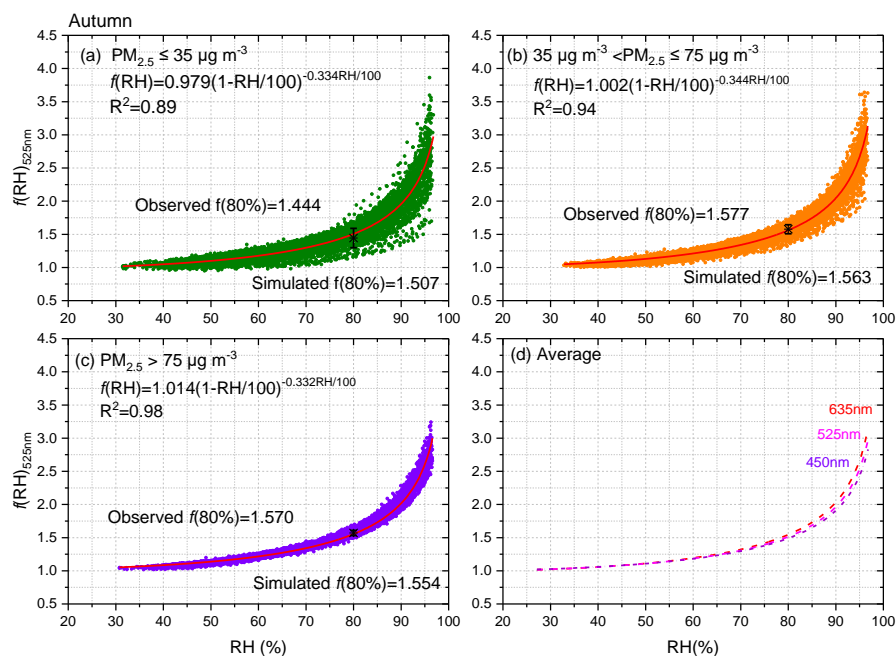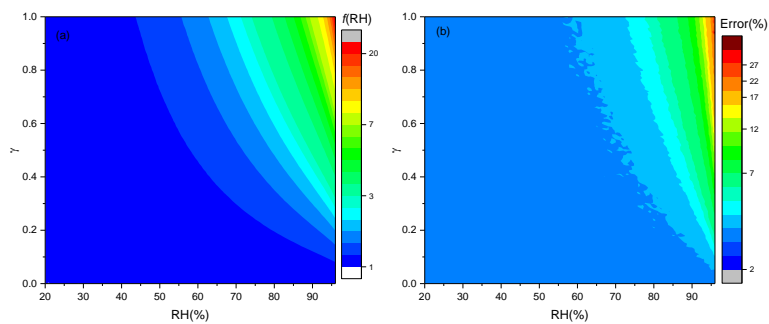
660

Figure 3

663
664

Figure 4

665
666
Figure 5

667
668
Figure 6

669

670   Figure 7

671